Journal of Electroanalytical Chemistry 895 (2021) 115401

Contents lists available at ScienceDirect

Journal of Electroanalytical Chemistry

journal homepage: www.elsevier.com/locate/jelechem

Facile microwave synthesis of cerium oxide@molybdenum di-sulphide@reduced graphene oxide ternary composites as high performance supercapacitor electrode

P. Stephen Selvamani [a], J. Judith Vijaya [a,*], L. John Kennedy [b], B. Saravanakumar [c], N. Clament Sagaya Selvam [d], P. Joice Sophia [e]

[a] Catalysis and Nanomaterials Research Laboratory, Department of Chemistry, Loyola College, University of Madras, Chennai 34, India
[b] Materials Division, School of Advanced Sciences, Vellore Institute of Technology University, Chennai Campus, Chennai 127, India
[c] Department of Physics, Dr. Mahalingam College of Engineering and Technology, Pollachi, India
[d] School of Chemical Engineering, Sungkyunkwan University, Suwon 16419, Republic of Korea
[e] Centre for Advanced Materials, Aaivalayam-DIRAC, Coimbatore 046, India

ARTICLE INFO

Keywords:
Nanocomposites
Microwave synthesis
Layered materials
Supercapacitor

ABSTRACT

There is a huge requirement for renewable energy resources to avoid the usage of fossil fuel attracted the researchers to work on the energy storage devices, such as supercapacitors. Herein, the novel synthesis of CeO_2@MoS_2@rGO (CeMG) ternary composite by two step microwave synthetic route that will be employed as an outstanding electrode material for supercapacitor. In particular, the morphology studies confirm that the cerium oxide has spherical morphology with the controlled size in the range of 12–15 nm embedded with the layered sheets of MoS_2 and reduced graphene oxide. The CeMG composites exhibit excellent specific capacitance of 635 F g^{-1} which is achieved at the current density of 1 A g^{-1} compared to the pure CeO_2. In addition, prolonged cyclic stability with 88.9% capacitance is retained after 10,000 cycles of charging and discharging.

1. Introduction

The urgency in realizing the sustainable energy sources to address the demands of continuous growth in population and environmental pollution can be complimented by employing supercapacitor (SC) in energy storage applications [1]. Supercapacitors are the electrochemical capacitors having fascinating characteristics such as immense power and energy density, cost-efficient, eco-friendly, attractive recyclability, high cyclic stability and stable charging/discharging behaviour as compared with the classical energy storage devices, namely, batteries [2,3]. SC are the promising sustainable energy source with the extended commercialization in various fields of military equipment, advanced hybrid vehicles, movable electronic devices, wearable electronic device, electrical vehicles and backup in power supply [4].

The main classification of supercapacitor depends on the charge transfer mechanism: electrochemical double layer capacitors (EDLC) and pseudocapacitors. On the basis of charge transfer mechanism, the charge is deposited on the electrode-electrolyte interfaces for EDLC and the charge is transferred through faradaic reduction-oxidation reactions for the pseudocapacitors [5,6]. The pseudocapacitors possess higher storage capacity and energy density than that of EDLC. The transition metal oxides and the rare earth (RE) oxides are the well-being source of pseudocapacitors. The conventional transition metal oxides such as NiO [7], Co_3O_4 [8], Fe_2O_3 [9], MnO_2 [10], ferrites [11] and bimetallic oxides [12] etc. are reported as the pseudocapacitors, and recently researchers are focussing on RE metal oxide because of compact size, effects of interface, safe environment and large surface area [13]. Also, they have cost-efficiency, earth abundance and attractive electrochemical redox behaviour. In recent years, cerium oxide (CeO_2) is of great interest among all the RE metal oxides [14].

Two approaches that could mainly improve the performance of supercapacitor are: (i) Tuning the electrode materials thereby improving its surface area, enhanced porosity, improved redox activity and electrical conductivity in order to attain the optimal specific capacitance [15]. (ii) Designing the hybrid supercapacitor by combining two different electrodes is carried out to maximise the operating voltage [16]. Currently, the researchers are attracted towards the fine tuning of electrode materials by improving the surface area of the material, electrode-electrolyte interfaces, charge density, cyclic behaviour and electrical conductivity of the electrode materials [17]. This

* Corresponding author.
E-mail addresses: judithvijaya@loyolacollege.edu, jjvijaya78@gmail.com (J.J. Vijaya).

https://doi.org/10.1016/j.jelechem.2021.115401
Received 20 April 2021; Received in revised form 20 May 2021; Accepted 20 May 2021
Available online 23 May 2021
1572-6657/© 2021 Elsevier B.V. All rights reserved.

approach of enhancement is feasible by combining the layered graphene and transition metal dichalcogenides (TMD) materials with the metal oxides that could further boost the specific capacitance and pseudocapacitance behaviour [18,19]. Notably, two dimensional (2D) layered materials, such as graphene and TMD molybdenum disulphide (MoS_2) are potential candidates studied widely owing to their large surface area, easy passage of ions and improved electronic properties [20,21]. On the other hand, MoS_2 shows lower capacitance at the high applied current density, due to its stacked layer of S-Mo-S, weak ionic and electronic conductivity. To overcome this issue, MoS_2 binded with other 2D layered materials could be suggested for the betterment of the electrochemical performance [22], wherein reduced graphene oxide is found to be suitable evidenced from its excellent conductivity and stability towards the charge transfer [23,24].

Furthermore, the bandgap of CeO_2 nanoparticles could be shortened with the addition of graphene or reduced graphene oxide which will be useful to overcome the disadvantage of oxygen vacancy defects [1]. From recent studies, MoS_2-graphene composites demonstrated better SC performance with their improved specific capacitance, flexibility, cyclic stability, and high conductance by eliminating the disadvantage of the single counterpart [25–27]. Numerous synthetic methods such as hydrothermal [28], sonochemical [29], microwave assisted sol-gel synthesis [30] and solution processing techniques [31] are adopted for the synthesis of RE metal oxides. However, microwave synthesis is of keen interest, because of its exquisite environmental friendliness, low cost of investment, enhanced product quality with the removal of unwanted side products, facile operation and synthetic route [32].

The present work is aimed at the cost effective and cleaner microwave synthesis of CeO_2@MoS_2@rGO (CeMG) ternary composites. To the best of our knowledge, this is the first time to report the proposed nanocomposite combination using microwave synthesis and the as-prepared CeMG composite evidenced its suitability for electrode materials in supercapacitor application. The obtained result corroborates that the CeMG composite exhibits outstanding SC performance with high specific capacitance and long term stability. The reduced graphene oxide acts as the bridging material for the transfer of electrons in between the spherical CeO_2 nanoparticles and the layered MoS_2 for the enhancement of SC performance.

2. Materials and methods

We have purchased all the chemicals including metal precursors, reducing agent etc. chemicals used in the synthesis process from Merck Company. The graphite powder and chemicals needed for the electrode preparation (carbon black, polyvinylidene fluoride (PVDF)) were procurred from Alfa Aesar Company.

2.1. Synthesis of binary MoS_2/reduced graphene oxide (MG) composite

Graphene oxide was prepared using improved Hummers method [33]. In detail, the graphene oxide solution (GO) was made by dispersing (10 mg/mL) in distilled water by working on the bath and probe sonication for 15 min each. The 50 mL aqueous solution containing sodium molybdate (1 mM) and thiourea (5 mM) was taken in one beaker and prepared GO solution was taken in the another beaker added slowly to the above mixture. It was agitated continuously to attain the homogenous mixture followed by transfer of solution into the crucible and kept in household microwave oven for 10 min with the operating frequency of 2.45 GHz and power of 700 W. The black powder of binary MoS_2/rGO composites was obtained after washing several times with distilled water, ethanol, centrifuged at 3000 rpm and dried in the hot air oven at 80 °C for 12 h [34].

2.2. Synthesis of CeO_2/MoS_2/rGO (CeMG) ternary composite

About, 0.1 M of cerium (III) nitrate hexahydrate ($Ce(NO_3)_3{\cdot}6H_2O$) was dissolved in 70 mL of distilled water, small amount of MG composite was added slowly and the above mixture was stirred vigorously for 20 min to attain the homogeneous layer. Consequently, 10 mL of freshly prepared solution of 0.05 M of NaOH was slowly added to the above mixture with continuous stirring for 30 min. Finally, the mixed solution was transported into the crucible, kept in a microwave oven for 10 min and the obtained yellowish grey powder was subsequently washed several times with distilled water and ethanol. The prepared CeMG composite was calcined at 600 °C for 3 h for the complete conversion of ceric hydroxide into cerium oxide. The cerium oxide (CeO_2) was prepared by the similar above-mentioned procedure by eliminating the step addition of MG composite.

2.3. Characterization

The high resolution scanning electron microscopy (HRSEM) images were recorded using FEI-Quanta FEG 200F and Transmission electron microscopy (TEM) images were obtained from the FEI Tecnai 20 model at the accelerating voltage of 200 kV to understand the detailed information about the structural and morphological behaviour of the CeMG composites. X-ray diffraction (XRD) patterns were measured with the help of Bruker D8 diffractometer with CuKα, λ = 1.5406 Å.

2.4. Working electrode preparation

The CeMG working electrode was prepared by blending the active material (80%), 10% of polyvinylidene fluoride (PVDF) as a binder, 10% carbon black, and made into homogenous slurry using *N*-methyl pyrrolidone (NMP) as the solvent. Prior to the coating of active material on the nickel foam (Ni-Foam), the Ni-foam is cleaned using distilled water and isopropyl alcohol in an ultra-sonication bath. Then, the slurry was coated on the cleaned Ni-foam (current collector) within the area of 1 cm × 1 cm. Finally, the working electrode was dried in a hot air oven at 80 °C for 6 h to remove the excess solvent. The mass loading of active material on the nickel foam was controlled to 2 mg cm^{-2} including binder.

2.5. Electrochemical measurements and its calculations

The electrochemical performance of the pure CeO_2 and CeMG composite were determined using cyclic voltammetry (CV), galvanostatic charge–discharge (GCD) and electrochemical impedance spectroscopy (EIS) and cycling stability studies. All the electrochemical studies were performed in the CHI660C electrochemical workstation utilizing three-electrode configuration. The CeMG composites coated on the nickel foam, platinum wire and Ag/AgCl were used as the working, counter and reference electrode respectively. An aqueous solution of 6 M KOH was used as the electrolytic solution. The specific capacitance of the electrode materials was determined from CV curves with the following equation

$$C_{sp} = \frac{\int I \times dV}{m \times \nu \times \Delta V} \ (or)\ C_{sp} = \frac{Area}{m \times \nu \times \Delta V} \quad (1)$$

where C_{sp} is the specific capacitance (F g^{-1}), I is the discharge current, m is the active mass of the electrode material (g),ν is the potential scan rate (V s^{-1}), ΔV is the operating discharge potential range (potential window) and the area of the curve is calculated from the obtained CV curve (in AV units).

The specific capacitance was determined using the GCD curve using the following equation

$$C_{sp} = \frac{I\Delta t}{m\Delta V} \quad (2)$$

where Csp represents the specific capacitance (F g^{-1}), Δtis the time taken for the charge-discharge (s), m is the mass of the active materials loaded on the electrode (mg cm^{-2}) and ΔV is the potential window of GCD curve.

3. Results and discussion

3.1. X-ray diffraction analysis

The characteristic crystalline nature, average crystallite size and the purity of the prepared sample can be examined by XRD analysis. Fig. 1(a), (b), (c) and (d) represents the XRD pattern of rGO, MoS_2, pure CeO_2 and CeO_2@MoS_2@rGO (CeMG) composites, respectively. The XRD pattern (Fig. 1(a)) of rGO shows the peak value at 2θ value of 25.7° corresponds to the (002) plane of rGO. The XRD pattern of MoS_2 perfectly matches with the JCPDS card No. 01-070-9264 and the peak positioned at 2θ values of 14.2°, 33.2°, 39.4° and 58.8° confirms the presence of miller indices planes of (002), (100), (103) and (110), respectively. The XRD spectrum of CeMG ternary composites was compared with the pristine CeO_2, rGO and MoS_2 to verify the formation and purity of the samples. Notably, both the XRD spectrum evidenced the same diffraction peak at the 2θ values of 28.7°, 33.3°, 47.5°, 56.5°, 59.3° and 69.9° in agreement with the cubic crystals planes of miller indices (111), (200), (220), (311), (222) and (400) correspondingly. The achieved results revealed that the XRD pattern resembles with the JCPDS card no. 01-0800 of CeO_2 with the space group of *Fm*-3*m*. Furthermore, the other peaks present at the 2θ values of 25.7°, 14.5° and 33.2° indicated the (002) plane of reduced graphene oxide, (002) and (100) planes of MoS_2, correspondingly. As compared with the pure CeO_2, the peak intensity of the CeMG composite was reduced after the addition of MoS_2/rGO binary composite. The absence of other peaks of rGO and MoS_2 components are mainly ascribed to the addition of small amount of the as-prepared sample [35]. The crystallite size of CeO_2 particles was determined using Debye Scherrer formula

$$D = 0.89\lambda/\beta\mathrm{Cos}\theta \quad (3)$$

wherein, D represents the crystallite size, λ-wavelength of X-rays, θ-Bragg's diffraction angle and β-full width at half maximum (FWHM) of the diffraction peak [36]. The calculated crystallite size of CeO_2 nanoparticles was in the range of 12–18 nm for both the pristine CeO_2 and CeMG composites. It confirms the uniformity in crystallite size and morphology of the CeO_2 nanoparticles samples before and after the formation of composites.

3.2. Morphological analysis

The surface appearance morphology of the CeMG composite was investigated by HR-SEM and TEM images. Fig. 2(a), (b), (c) and (d) portrays the HR-SEM image of CeO_2, MoS_2, MoS_2@rGO and CeMG composite, respectively. The HRSEM image of pristine CeO_2 (Fig. 2 (a)) confirms the spherical morphology of CeO_2 nanoparticles. The HRSEM image of MoS_2 (Fig. 2(b)) and MoS_2@rGO (Fig. 2(c)) substantiates that both the MoS_2 and rGO are in sheet-like morphology. The HRSEM image of CeMG composites demonstrates that the spherical CeO_2 nanoparticles that are well ingrained into the matrix of the binary composite MoS_2 and rGO. The microwave synthesized CeMG composites are in the combined and well-organized form as the spherical CeO_2 nanoparticles are completely covered with the sheet-like morphology of the rGO.

Fig. 3 displays the HRTEM image of CeMG composite and the HRTEM results affirm that the CeO_2 nanoparticles are homogenous with uniform spherical morphology having average particle size in the range of 12–15 nm in diameter (calculated using the ImageJ software). HRTEM image (Figs. 3(a) and 1s (Supplementary)) confirms the spherical nanoparticles of CeO_2 wrapping up the two different types of flakes corresponding to rGO and MoS_2 having soft sheets and flower like sheets, respectively which is in well agreement with the HRSEM images. The resulting particle size examined from the HRTEM is in agreement with the crystallite size calculated from the XRD spectrum [37]. The two different alignments of lattice fringes are observed due

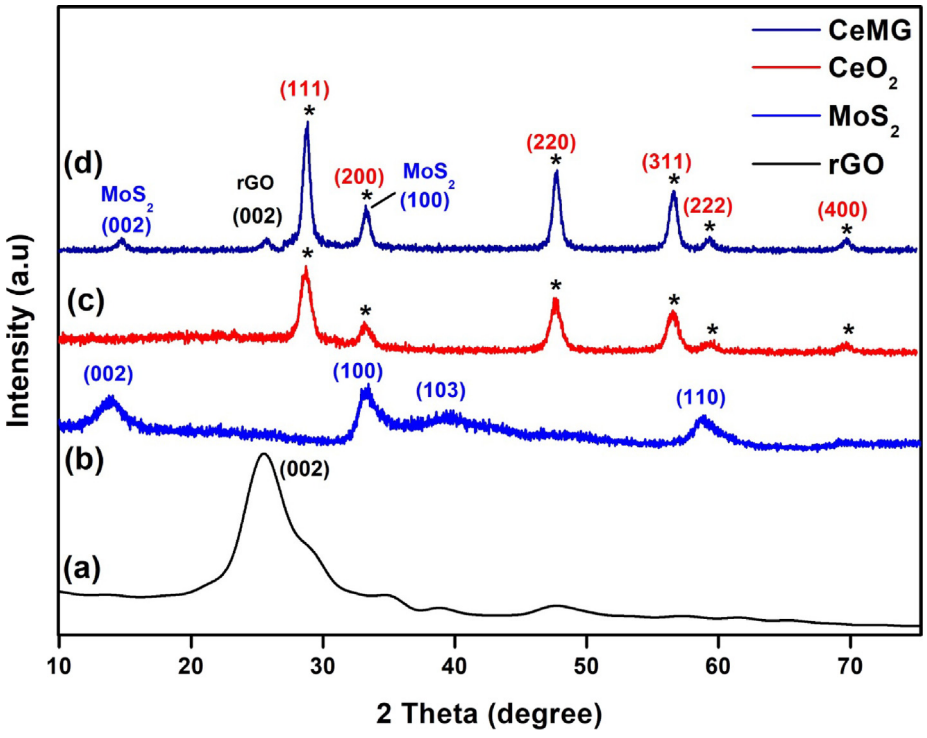

Fig. 1. XRD pattern of (a) rGO (b) MoS_2 (c) pure CeO_2 and (d) CeO_2@MoS_2@rGO (CeMG) composite.

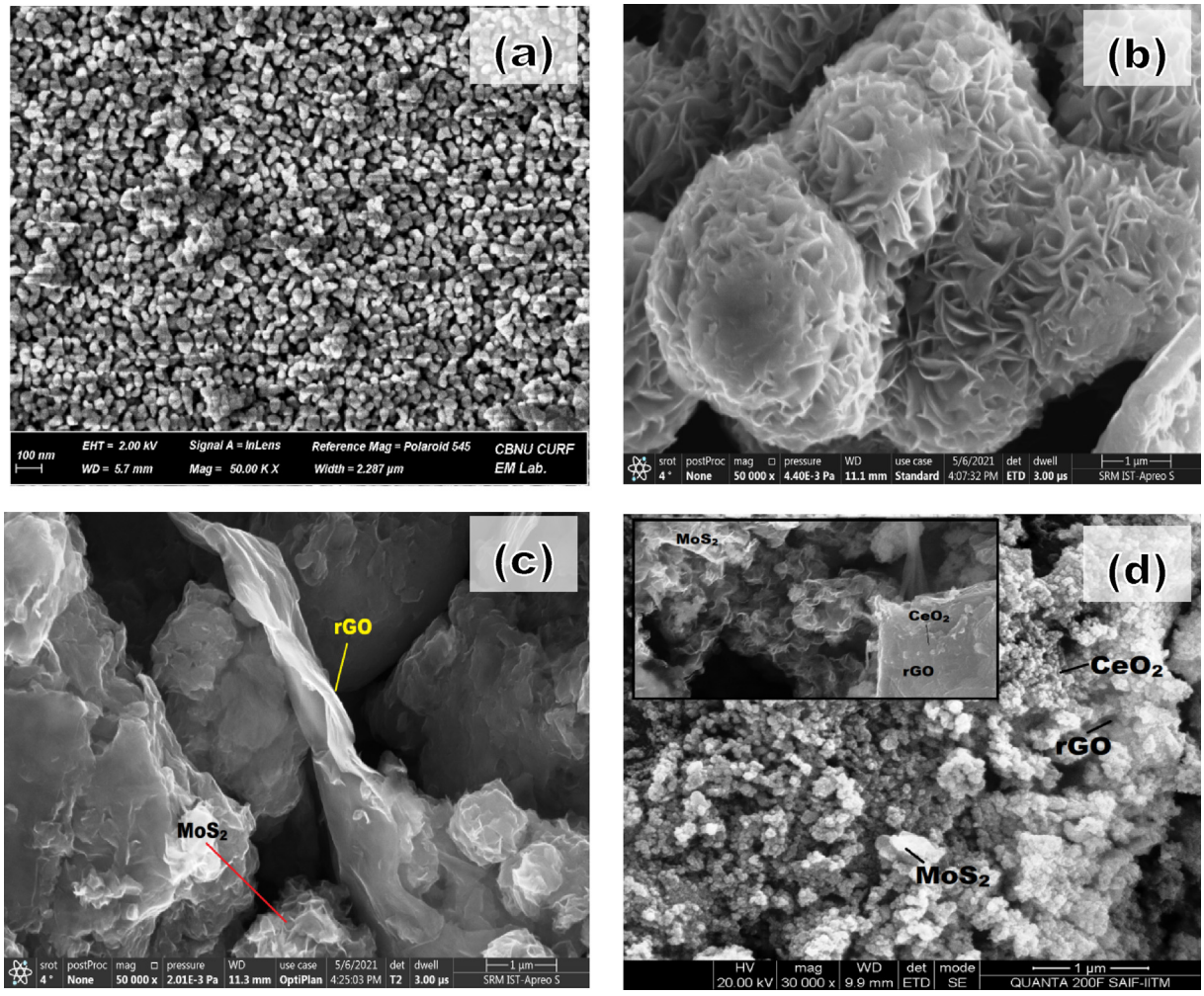

Fig. 2. HR-SEM image of (a) CeO_2 (b) MoS_2 (c) MoS_2@rGO (d) CeMG composite.

to the interplanar spacing for (1 1 1) plane of CeO_2 nanoparticles (horizontal alignment of Ca. 0.303 nm), the interplanar spacing of (1 0 0) plane of MoS_2 (horizontal alignment of Ca. 0.274 nm) and interplanar spacing of (0 0 2) plane of rGO (vertical alignment of Ca. 0.382 nm). In comparison with the alternative methods such as wet chemical, hydrothermal and thermal decomposition synthesis of CeO_2, microwave methods of synthesis yield CeO_2 nanoparticles with uniform structure and spherical shape [32]. Additionally, the HRTEM image confirms that the particles are combined together leading to the formation of porous morphology (Fig. 3(b)) [38].

The selective area electron diffraction (SAED) analysis is a tool that confirms the purity of the composites based on the crystalline structure. The SAED pattern of the CeMG composites is given in Fig. 3(a) inset. The attained spots in the SAED pattern reflects the miller indices planes (1 1 1), (2 0 0), (2 2 0), (3 1 1), (4 0 0), (3 3 1), (4 2 0) and (4 2 2) of CeO_2 and is in accordance with the diffraction pattern as obtained in the XRD spectrum with the JCPDS card no. 01-0800. Notably, the d-spacing of CeMG composites exactly matches with the d-spacing of CeO_2. Furthermore, the (1 0 0) plane of MoS_2 and (0 0 2) plane of rGO is also observed in the SAED pattern of CeMG composites.

The energy dispersive X-ray spectroscopic (EDX) analysis confirms the purity of the sample and showed the presence of elements namely, cerium (Ce), oxygen (O), molybdenum (Mo), sulphur (S) and carbon (C) in K-series as shown in Fig. 4. Notably, no other elemental peak is present in the EDX analysis certifying the purity of composites in which the carbon peak is attributed mainly due to the presence of rGO (sheets of carbon). The existence of Mo and S confirms the formation of the MoS_2. The EDS spectrum of CeMG composites reveals that the weight percentage of the elements such as Ce, C, O, Mo and S are 51.37%, 37.21%, 7.31%, 3.97% and 0.12%, respectively. This corroborates the presence of excess CeO_2 and rGO and limited quantity of MoS_2. The results clearly affirm the purity and the formation of ternary composites with the CeO_2, rGO and MoS_2.

3.3. Electrochemical studies of CeMG composites

3.3.1. Cyclic voltammetry

The CV curves (potential window of 0–0.7 V) of the pure CeO_2 and CeMG composites in the Fig. 5(a) indicate the presence of well-defined oxidation and reduction peaks, thus assuring the redox behaviour of the samples at 100 mV s^{-1}. In addition, the peak broadening of CV curve for CeMG composite indicate that the addition of the MoS_2@rGO binary composites with the cerium oxide significantly enhances the capacitive behaviour of the material. Fig. 5(b) indicates the CV curve with the variation in the potential scan rates of 10–100 mV s^{-1}. The calculated specific capacitance is found to be 550, 436.8, 374.3, 330.6, 296.6, 271.7, 249.6, 231.2, 214.7 F g^{-1} and 202.6 F g^{-1} with the variation in scan rate from 10 mV s^{-1} to100 mV s^{-1} respectively are shown in the Table 2. Further, the curves in Fig. 5(b) with different voltage sweep rates showed the shift of anodic and cathodic peak potential to the higher and lower potential respectively. At the lower scan rate, there is a proper circulation of electrolyte ions (K^+ ions) into

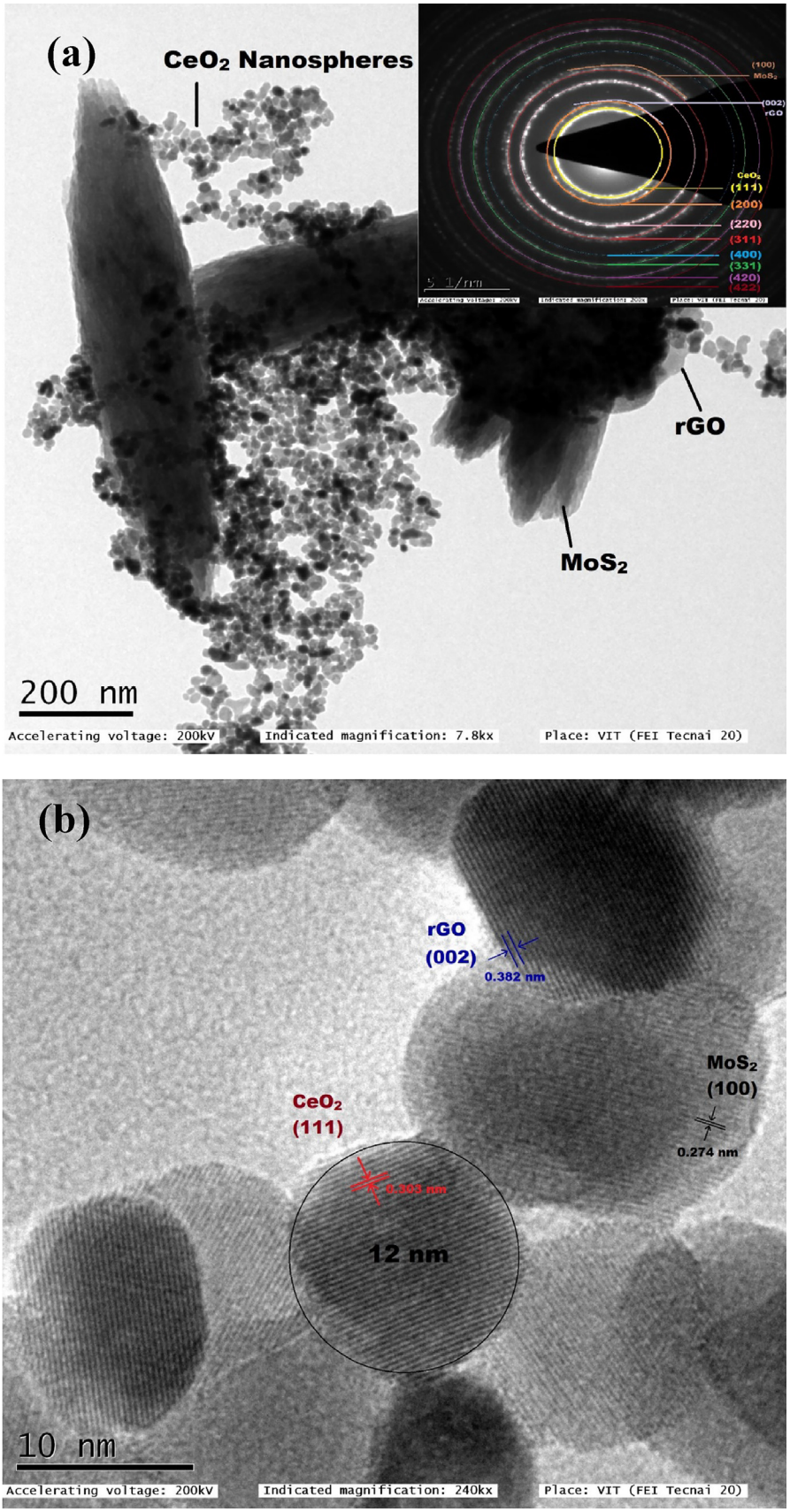

Fig. 3. (a, b) HR-TEM images of CeMG composite (3(a) Inset: SAED pattern of CeMG composite).

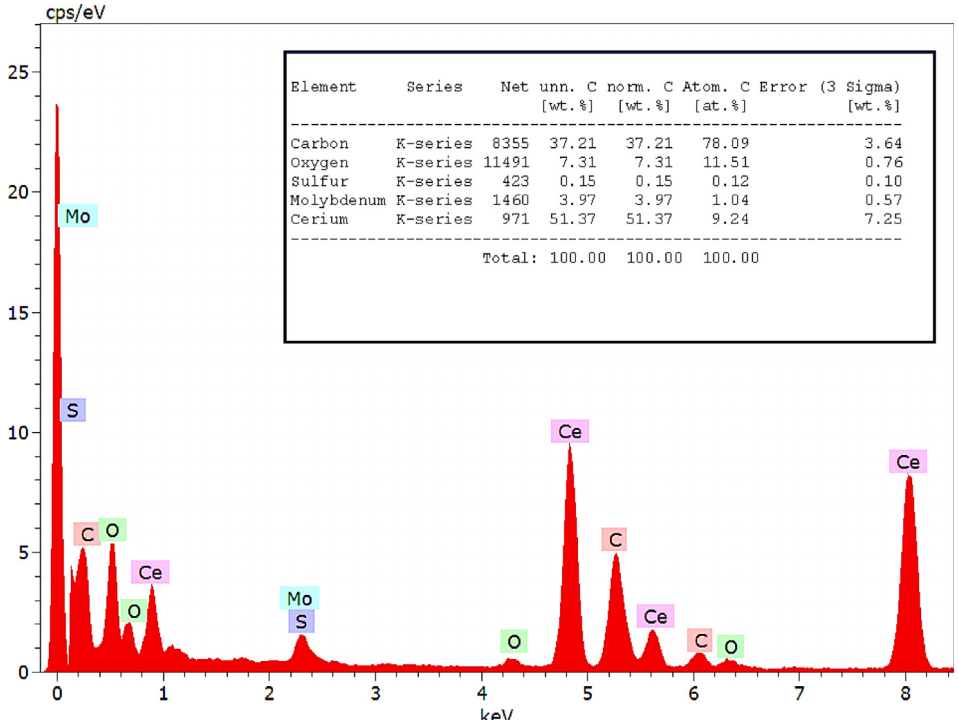

Fig. 4. EDX analysis of CeMG composite.

the interior electrode surface that leads to higher capacitance. Notably, at the higher scan rate, the movements of the electrolyte ions were blocked by its surface, enhanced reversible redox potential and outer surface of the electrode alone involved in the charge storing process [39,40].

The entire sweep rates having the pair of redox peaks was observed that attributes to redox conversion of Ce^{3+}/Ce^{4+} with the possibilities of adsorption/desorption of K^+ ions on the surface of electrode and the possibility of intercalation/deintercalation of K^+ ions into or away from the surface of CeO_2 and the possible faradaic and non-faradaic reactions are indicated in the following equation [41,42]:

$$\text{Non-Faradaic Reaction}: \ CeO_2(\text{at Surface}) + K^+ + e^- \leftrightarrow (CeO_2.K^+) \text{ at surface} \quad (5)$$

$$\text{Faradic Reaction}: Ce^{IV}O_2 + K^+ + e^- \leftrightarrow (Ce^{III}O.OK) \text{ Intercalation} \quad (6)$$

As compared, the specific capacitance calculated for the CeMG composites (202.6 F g^{-1}) with the pure CeO_2 (73.5 F g^{-1}) at the scan rate of 100 mV s^{-1} is predominantly higher and this confirms the addition of MoS_2@rGO composite to the pure CeO_2 nanospheres enhanced the electrochemical behaviour.

3.3.2. Galvanostatic charge-discharge

Galvanostatic charge-discharge measurements are playing a vital role in the determination of capacitive behaviour of the electrode materials. The GCD analysis of pure CeO_2 and CeMG composites were measured with the potential window of 0–0.4 V for different current densities (1–10 A g^{-1}). The GCD profiles of CeO_2 and CeMG samples at the current density of 1 A g^{-1} are presented in the Fig. 6(a). It is interesting to note that the CeMG electrode shows higher discharge time compared to the pure sample. This behaviour is attributed to the addition of the MoS_2/rGO composites with the CeO_2 which notably raised the capacitance of the bare sample. Interestingly, CeO_2 and MoS_2 have similar functionality in terms of supercapacitor application. For the better performance, high electrical pathway material such as rGO is introduced to replace the properties of CeO_2 or MoS_2 for the formation the ternary electrode material [43]. Fig. 6(b) shows the GCD curves of CeMG composite for the different applied current density of 1–10 A g^{-1}. The charge-discharge behaviour of the CeMG composite is not symmetrical that might be ascribed to the reaction between the CeO_2 and the aqueous KOH electrolyte solution in the lowest applied current density [44]. The calculated specific capacitance values (using Eq. (2)) are found to be 635, 375, 326.2, 300, 291.9, 250.3, 245.8, 236.3 F g^{-1} and 227.5 F g^{-1} for the applied current density from 1 A g^{-1} to 10 A g^{-1} respectively. The calculated values of the specific capacitance are listed in the Table 3. The specific capacitance calculated from GCD curve closely resembles the specific capacitance calculated from the CV curves. Notably, there is a constant decrease in the specific capacitance observed with the increasing current density and the high specific capacitance of 635 F g^{-1} is attained for the current density of 1 A g^{-1}.

The performance of the CeMG composites are compared with the other reported CeO_2 based composites and indicated in the Table 1. Notably, the calculated capacitance value for CeMG composite is 635 F g^{-1} at 1 A g^{-1}. Meanwhile, CeO_2 combined with the graphene or rGO exhibits the specific capacitance of 280 F g^{-1} which confirms that the addition of MoS_2 to the CeO_2/rGO composites enhances the specific capacitance and improves the cycle life [21,45]. Vanitha et al., [19] demonstrated that ternary Ag/CeO_2/rGO composites exhibit the specific capacitance of 710.42 F g^{-1} at the lowest applied current of 0.2 A g^{-1}. Moreover, the excellent electrical conductivity of the layered and carbon-based materials (rGO, CNT) will boost the specific capacitance by acting as a good electrical junction between the particles [46]. As compared with the reported, the present work manifests the excellent specific capacitance and cyclic stability.

3.3.3. Electrochemical impedance spectroscopy

Electrochemical impedance spectroscopy (EIS) is the key investigation to understand the capacitive and resistive properties of electrode materials. EIS is the predominant technique to examine the kinetics of the charge transfer that occurs at interface of electrode/electrolyte and the properties, such as transport of ions and electrical conductance of

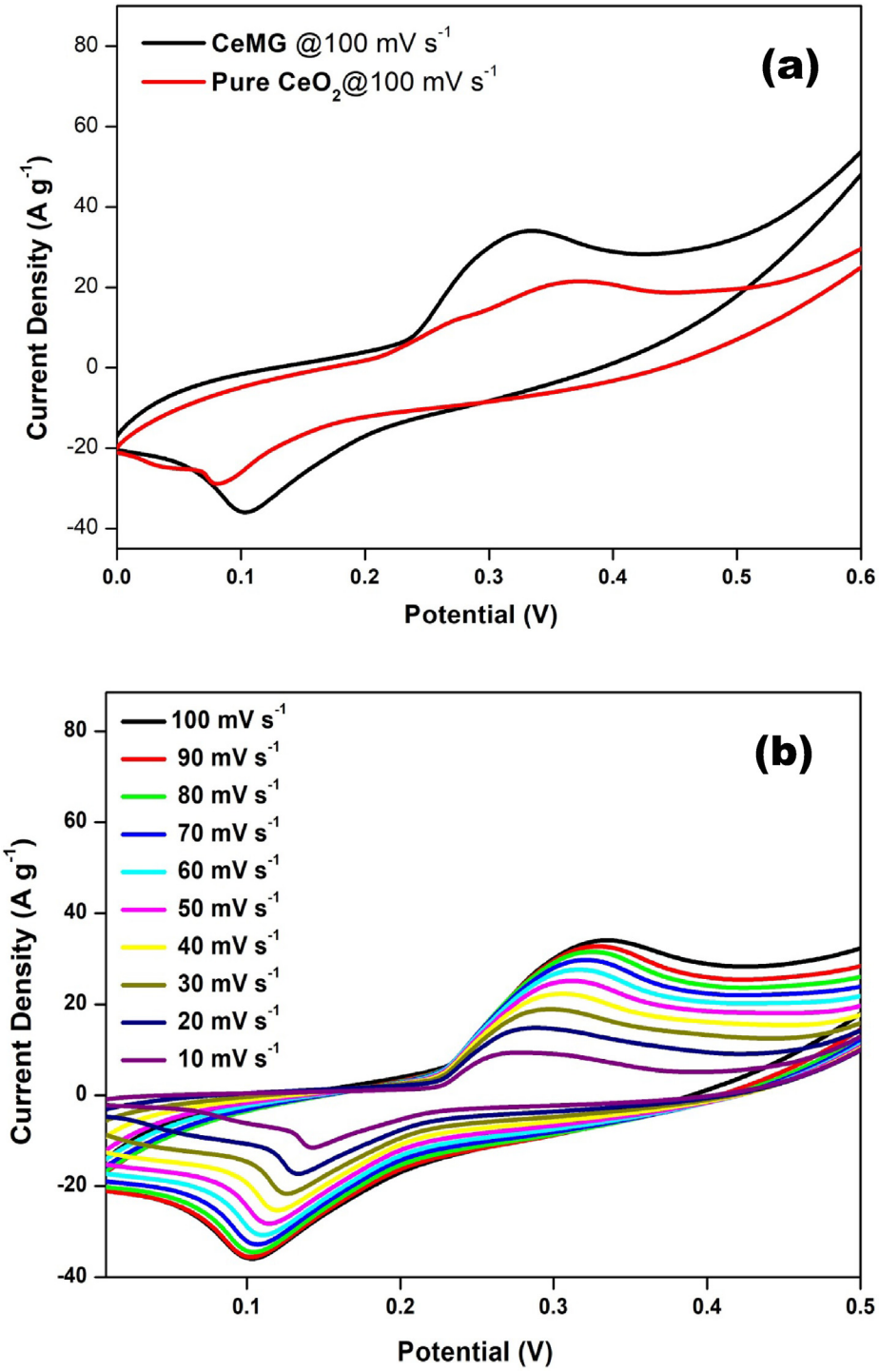

Fig. 5. (a) Comparative CV curve of CeMG and CeO_2 at the voltage sweep rate of 100 mV s^{-1} (b) CV curve of CeMG working electrode at different voltage sweep rates.

Table 1
Comparison of electrochemical behaviour of CeMG with other reported literatures.

Active material	Electrolyte	Potential Window (V)	Specific capacitance	Cyclic stability	References
CeO_2/rGO composite	3 M KOH solution	0–0.4	282 F g^{-1} at 2 A g^{-1}	86% retained after 1000 cycles at 2 A g^{-1}	[41]
CeO_2/Fe_2O_3	2 M Na_2SO_4	−0.8 to 0	158 F g^{-1} at 0.5 A g^{-1}	87.5% retained after 2000 cycles at 200 mV s^{-1}	[53]
CeO_2/rGO	2 M KOH	0–0.5	280 F g^{-1} at 1 A g^{-1}	98% retained after 5000 cycles	[42]
CeO_2/MWCNT	6 M KOH	0–0.45	455.7 F g^{-1} at 1 A g^{-1}	81.1% retained after 2000 cycles at 10 A g^{-1}	[54]
Ag/CeO_2/ rGO	3 M KOH	−0.2 to 1	710.42 F g^{-1} at 0.2 A g^{-1}	Slight changes after 1000 cycles at 0.2 A g^{-1}	[43]
CeO_2/MoS_2/rGO	6 M KOH	0–0.4	635 F g^{-1} at 1 A g^{-1}	88.9% retained after 10,000 cycles at 20 A g^{-1}	Present Work

Table 2
Specific capacitance of CeMG electrode calculated from cyclic voltammetry (CV).

Scanrate	10 mV s^{-1}	20 mV s^{-1}	30 mV s^{-1}	40 mV s^{-1}	50 mV s^{-1}	60 mV s^{-1}	70 mV s^{-1}	80 mV s^{-1}	90 mV s^{-1}	100 mV s^{-1}
Specific capacitance from CV (F g^{-1})	550	436.88	374.31	330.63	296.61	271.66	249.58	231.19	214.67	202.62

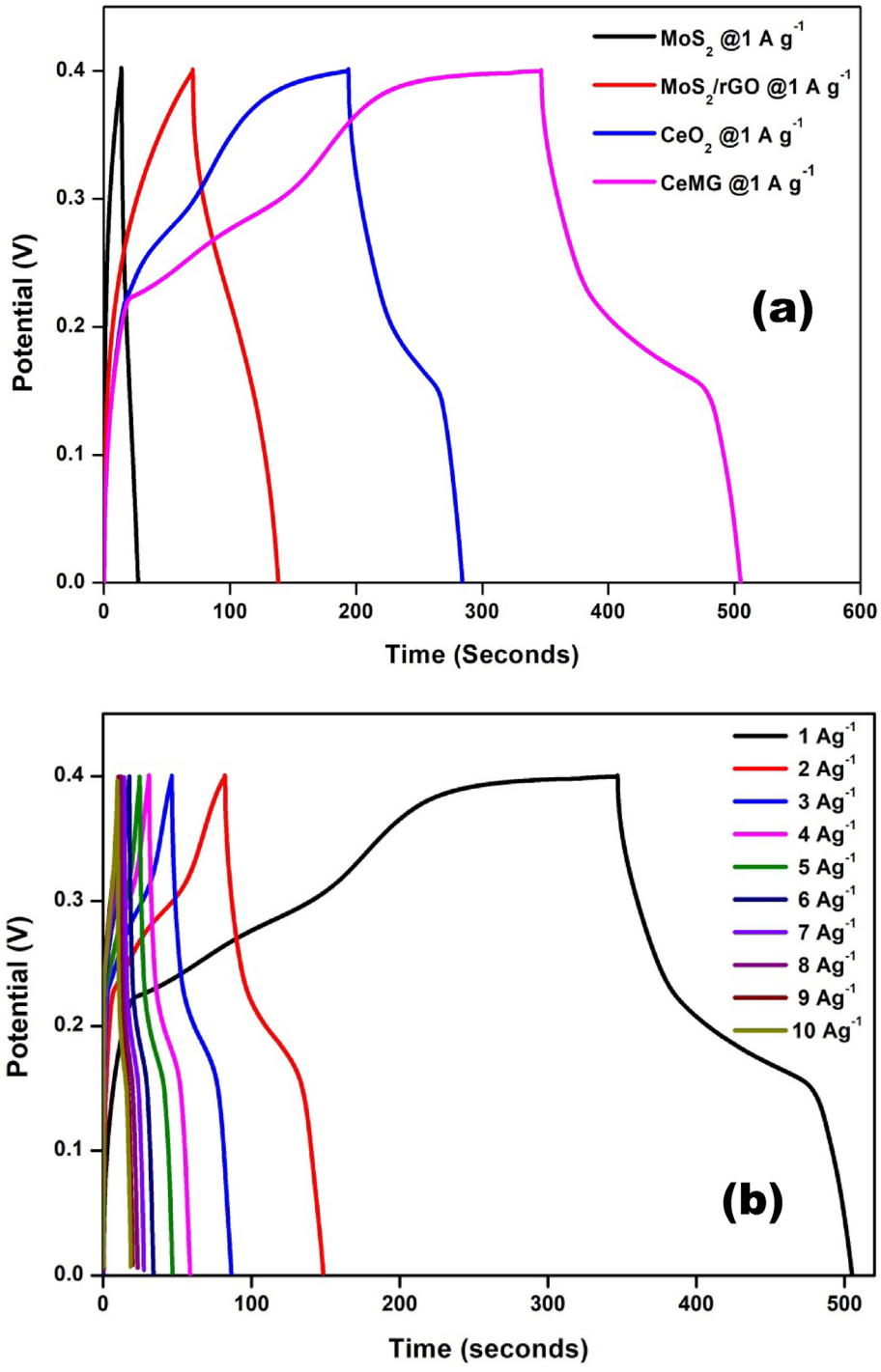

Fig. 6. (a) Comparative GCD curve of CeMG and CeO_2 at the applied current density of 1 A g^{-1} (b) GCD curve of CeMG working electrode at different applied current density.

the electrode material [47,48]. Fig. 7 represents the Nyquist plot with the real component Z′ (X-axis) against imaginary −Z″ (Y-axis) for the CeMG and pure CeO_2 as the electrode material with the Randles circuit (inset). The three significant regions in the Nyquist plot are high, middle and low frequency regions. The semicircle occurs at the high frequency region, the intersection of the semicircle and the 45° line

Table 3
Specific capacitance of CeMG electrode calculated from galvanostatic charge discharge (GCD) studies.

Current density	1 A g^{-1}	2 A g^{-1}	3 A g^{-1}	4 A g^{-1}	5 A g^{-1}	6 A g^{-1}	7 A g^{-1}	8 A g^{-1}	9 A g^{-1}	10 A g^{-1}
Specific capacitance from GCD (F g^{-1})	635	375	326.2	300	291.9	258.1	250.3	245.8	236.3	227.5

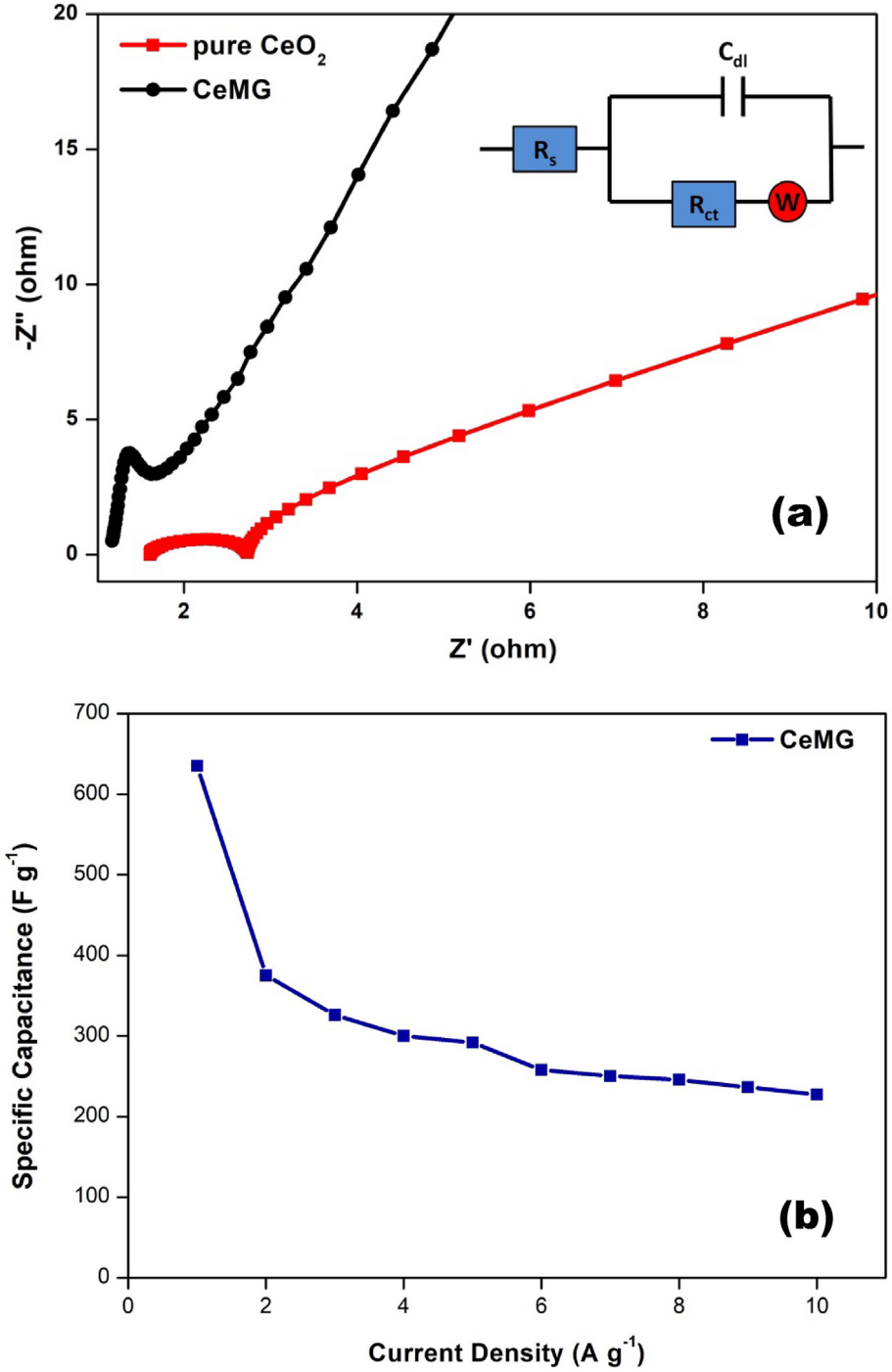

Fig. 7. (a) Nyquist plot of CeMG and pure CeO_2 as the working electrode material with the Randles circuit (inset) (b) Rate capability of CeMG electrode (specific capacitance Vs. current density).

occur in the middle frequency and the inclined line occurs at the low frequency region of the plot. The four resistive parameters, such as solution resistance (R_s), charge-transfer resistance (R_s), equivalent series resistance (ESR) and Warburg resistance (W) are the key factors analysed using the nyquist plot. The starting point of the semicircle is the R_s; the closing point of the semicircle is the R_{ct} and the slope of the 45° inclined line denotes W. The ESR is the difference between the charge transfer resistance and the solution resistance

Table 4
Observed resistance values of CeMG electrode from the electrochemical impedance studies.

Materials/Resistance	R_s (Ω)	R_{ct} (Ω)	ESR (Ω)	W (Ω)
CeO_2	1.576	2.758	1.182	‘4.714
CeMG	1.157	1.624	0.467	1.339

(ESR = R_{ct} − R_s). The calculated resistance are indicated in the Table 4. The calculated Rs value of CeMG (1.157 Ω) is lower than that of pure CeO_2 (1.576 Ω) owing to the lower resistance of the electrode to the KOH electrolytic solution. In agreement with the fitted data, the decreased value of R_{ct} value for CeMG (1.624 Ω) than pure CeO_2 (2.758 Ω) that gives rise to the improved charge-discharge by reducing the ion-diffusion path of CeMG electrode [49]. As compared with the resistivity behaviour of CeO_2 with the CeMG composites, CeMG composites manifest lower resistance values of R_s, R_{ct}, ESR and W than that of pure CeO_2. Furthermore, it confirms that the addition of rGO and MoS_2 to the CeO_2 improves the charge transfer properties and enhanced capacitive performance of the electrode materials.

3.3.4. Rate capability, cyclic stability, energy and power densities of CeMG electrode

Fig. 7(b) shows the rate capability curve of CeMG composites as calculated from the GCD measurements. It is also noted that the specific capacitance falls suddenly at the initial stage, followed by a steady decrease in the specific capacitance. Notably, the reduced capacitance observed for high current density is attributed mainly to the penetration speed of the K^+ electrolyte ions into the pores of electrode material thereby improving the development of electrostatic charge layer. However, in case of lower current density, there is huge time availability for the penetration of electrolytic ions with the increase in the number of active sites [50,51]. The cyclic stability is considered as an important property towards the commercialization of the electrode materials. Fig. 8 presents the cyclic stability behaviour such as percentage retained and the specific capacitance of the CeMG composite measured at the current density of 20 A g^{-1} with the potential window of 0–0.4 V. The cyclic stability results of CeMG composite indicates that the 88.9% of the initial capacitance is retained after 10,000 cycles of charge-discharge. At the initial stage, the calculated specific capacitance is found to be 183.5 F g^{-1} and the calculated specific capacitance after 10,000 cycles of charge-discharge is 160.5 F g^{-1}. The hump occurs during charging is on account of the increase in the applied current and also indicates the IR drop. Notably, the decrease in the specific capacitance is owing to the IR drop or the electrolytic solution resistance. The improved cyclic characteristics of the CeMG composite are owing to the addition of MoS_2 and rGO to the CeO_2 with enhanced active cites for the faster ion movement between the electrolyte and electrode material [52].

4. Conclusion

In concise, CeO_2@MoS_2@rGO ternary composite is synthesized using the facile and rapid microwave synthetic route and extend it to be the suitable electrode material for high performance supercapacitors application. The CeMG composite manifests the excellent specific capacitance of 635 F g^{-1} at the current density of 1 A g^{-1} in 6 M KOH electrolytic solution. Importantly, the CeMG as working electrode exhibits the extended cyclic stability with 88.9% capacitance is retained after 10,000 charging/discharging cycles. To our best knowledge, this is the first report on the CeO_2@MoS_2@rGO ternary composite as the working electrode for high performance supercapacitor applications. Finally, the results obtained for the CeMG composite confirms that the CeMG can be the suitable candidate for the effective fabrication of high performance supercapacitor and for future energy

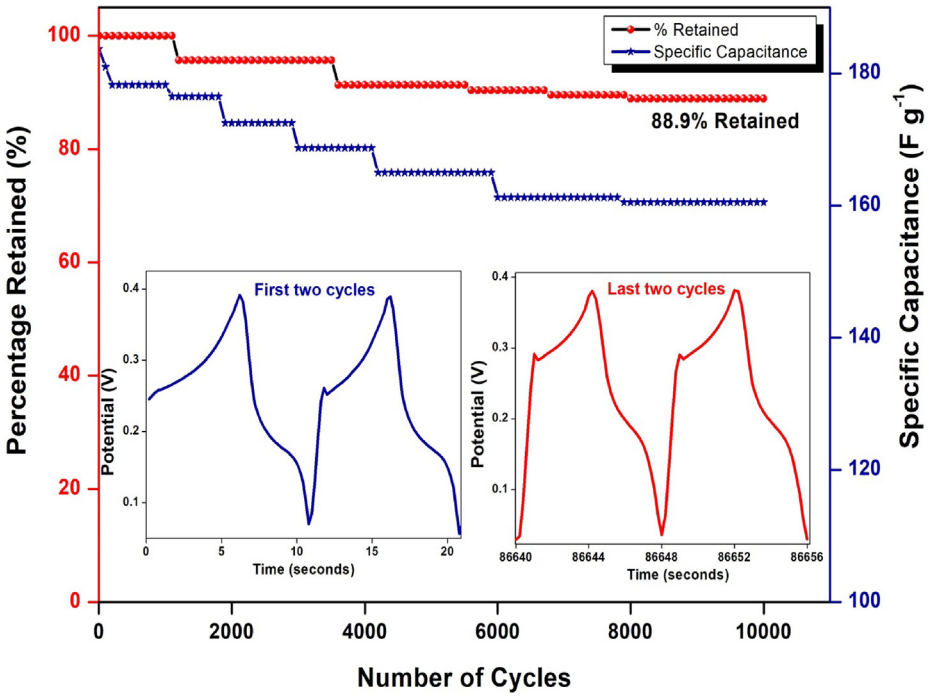

Fig. 8. Cyclic stability of the CeMG composite over 10,000 charging/discharging cycles at the current density of 20 A g^{-1}.

storage device with the excellent specific capacitance and the cycling behaviour.

CRediT authorship contribution statement

P. Stephen Selvamani: Validation, Investigation, Resources, Writing - original draft, Writing - review & editing, Visualization. **J. Judith Vijaya:** Methodology, Resources, Writing - original draft, Writing - review & editing, Visualization, Supervision. **L. John Kennedy:** Formal analysis. **B. Saravanakumar:** Investigation. **N. Clament Sagaya Selvam:** Validation. **P. Joice Sophia:** Writing - review & editing.

Declaration of Competing Interest

The authors declare that they have no known competing financial interests or personal relationships that could have appeared to influence the work reported in this paper.

Acknowledgement

The authors acknowledge the management of Loyola College, affiliated to University of Madras for offering the infrastructure to carry out the present work.

Appendix A. Supplementary data

Supplementary data to this article can be found online at https://doi.org/10.1016/j.jelechem.2021.115401.

References

[1] T. Saravanan, M. Shanmugam, P. Anandan, M. Azhagurajan, K. Pazhanivel, M. Arivanandhan, Y. Hayakawa, R. Jayavel, Facile synthesis of graphene-CeO_2 nanocomposites with enhanced electrochemical properties for supercapacitors, Dalton Trans. 44 (2015) 9901–9908.

[2] A. Rajapriya, S. Keerthana, C. Viswanathan, N. Ponpandian, Direct growth of MoS2 hierarchical nanoflowers on electrospun carbon nanofibers as an electrode material for high-performance supercapacitors, J. Alloy. Compd. 859 (2021) 157771.

[3] A. Zhang, L. Yue, D. Jia, L. Cui, D. Wei, W. Huang, R. Liu, Y. Liu, W. Yang, J. Liu, Cobalt/nickel ions-assisted synthesis of laminated CuO nanospheres based on Cu(OH)2 nanorod arrays for high-performance supercapacitors, ACS Appl. Mater. Interfaces 12 (2020) 2591–2600.

[4] T. Kim, E.P. Samuel, C. Park, Y. Kim, A. Aldalbahi, F. Alotaibi, S.S. Yoon, Wearable fabric supercapacitors using supersonically sprayed reduced graphene and tin oxide, J. Alloy. Compd. 856 (2021) 157902.

[5] W. Wei, B. Liu, Y. Gan, H. Ma, D. Chen, J. Qi, S. Li, One-step hydrothermal synthesis of Ni3S2/MoS2 nanocomposites on rGO: structural evolution and supercapacitor performance, Surf. Coat. Technol. 403 (2020).

[6] B. Zhang, X. Li, J. Zou, F. Kim, $MnCO_3$ on graphene porous framework via diffusion-driven layer-by-layer assembly for high-performance pseudocapacitor, ACS Appl. Mater. Interfaces 12 (2020) 47695–47703.

[7] S. Zhu, Y. Dai, W. Huang, C. Zhang, Y. Zhao, L. Tan, Z. Wang, In situ preparation of NiO nanoflakes on Ni foams for high performance supercapacitors, Mater. Lett. 161 (2015) 731–734.

[8] S. Vijayakumar, A.K. Ponnalagi, S. Nagamuthu, G. Muralidharan, Microwave assisted synthesis of Co_3O_4 nanoparticles for high-performance supercapacitors, Electrochim. Acta 106 (2013) 500–505.

[9] S. Yang, X. Song, P. Zhang, J. Sun, L. Gao, Self-assembled α-Fe_2O_3 mesocrystals/graphene nanohybrid for enhanced electrochemical capacitors, Small 10 (2014) 2270–2279.

[10] J.-G. Wang, Y. Yang, Z.-H. Huang, F. Kang, A high-performance asymmetric supercapacitor based on carbon and carbon–MnO_2 nanofiber electrodes, Carbon NY 61 (2013) 190–199.

[11] T. Arun, T. Kavin Kumar, R. Udayabhaskar, M.J. Morel, G. Rajesh, R.V. Mangalaraja, A. Akbari-Fakhrabadi, Size dependent magnetic and capacitive performance of $MnFe_2O_4$ magnetic nanoparticles, Mater. Lett. 276 (2020) 128240.

[12] S.G. Krishnan, M.H.A. Rahim, R. Jose, Synthesis and characterization of $MnCo_2O_4$ cuboidal microcrystals as a high performance psuedocapacitor electrode, J. Alloy. Compd. 656 (2016) 707–713.

[13] M. Isacfranklin, R. Yuvakkumar, G. Ravi, S.I. Hong, D. Velauthapillai, M. Thambidurai, C. Dang, T.S. Algarni, A.M. Al-Mohaimeed, Heterostructured $SmCoO_3$/rGO composite for high-energy hybrid supercapacitors, Carbon NY 172 (2021) 613–623.

[14] Q. Guo, J. Yuan, Y. Tang, C. Song, D. Wang, Self-assembled PANI/CeO_2/$Ni(OH)_2$ hierarchical hybrid spheres with improved energy storage capacity for high-performance supercapacitors, Electrochim. Acta 367 (2021) 137525.

[15] B. Saravanakumar, K.K. Purushothaman, G. Muralidharan, Interconnected V_2O_5 nanoporous network for high-performance supercapacitors, ACS Appl. Mater. Interfaces 4 (2012) 4484–4490.

[16] D. Tian, N. Song, M. Zhong, X. Lu, C. Wang, Bimetallic MOF nanosheets decorated on electrospun nanofibers for high-performance asymmetric supercapacitors, ACS Appl. Mater. Interfaces 12 (2020) 1280–1291.

[17] N. Padmanathan, S. Selladurai, Shape controlled synthesis of CeO_2 nanostructures for high performance supercapacitor electrodes, RSC Adv. 4 (2014) 6527–6534.

[18] Z. Ji, X. Shen, H. Zhou, K. Chen, Facile synthesis of reduced graphene oxide/CeO_2 nanocomposites and their application in supercapacitors, Ceram. Int. 41 (2015) 8710–8716.

[19] M. Vanitha, Keerthi, P. Cao, N. Balasubramanian, Ag nanocrystals anchored CeO_2/graphene nanocomposite for enhanced supercapacitor applications, J. Alloy. Compd. 644 (2015) 534–544.

[20] D. Kesavan, V.K. Mariappan, P. Pazhamalai, K. Krishnamoorthy, S.-J. Kim, Topochemically synthesized MoS_2 nanosheets: a high performance electrode for wide-temperature tolerant aqueous supercapacitors, J. Colloid Interface Sci. 584 (2021) 714–722.

[21] T. Li, H. Liu, A simple synthesis method of nanocrystals CeO_2 modified rGO composites as electrode materials for supercapacitors with long time cycling stability, Powder Technol. 327 (2018) 275–281.

[22] H. Wang, D. Tran, M. Moussa, N. Stanley, T.T. Tung, L. Yu, P.L. Yap, F. Ding, J. Qian, D. Losic, Improved preparation of MoS_2/graphene composites and their inks for supercapacitors applications, Mater. Sci. Eng., B 262 (2020) 114700.

[23] P. Hota, M. Miah, S. Bose, D. Dinda, U.K. Ghorai, Y.K. Su, S.K. Saha, Ultra-small amorphous MoS_2 decorated reduced graphene oxide for supercapacitor application, J. Mater. Sci. Technol. 40 (2020) 196–203.

[24] M. Saraf, K. Natarajan, S.M. Mobin, Emerging robust heterostructure of MoS_2-rGO for high-performance supercapacitors, ACS Appl. Mater. Interfaces 10 (2018) 16588–16595.

[25] J. Bao, X.-F. Zeng, X.-J. Huang, R.-K. Chen, J.-X. Wang, L.-L. Zhang, J.-F. Chen, Three-dimensional MoS_2/rGO nanocomposites with homogeneous network structure for supercapacitor electrodes, J. Mater. Sci. 54 (2019) 14845–14858.

[26] X. Jian, H. Li, H. Li, Y. Li, Y. Shang, Flexible and freestanding MoS_2/rGO/CNT hybrid fibers for high-capacity all-solid supercapacitors, Carbon NY 172 (2021) 132–137.

[27] L. Zhang, P. Cai, Z. Wei, T. Liu, J. Yu, A.A. Al-Ghamdi, S. Wageh, Synthesis of reduced graphene oxide supported nickel-cobalt-layered double hydroxide nanosheets for supercapacitors, J. Colloid Interface Sci. 588 (2021) 637–645.

[28] A.P.B. dos Santos, T.C.M. Dantas, J.A.P. Costa, L.D. Souza, J.M. Soares, V.P.S. Caldeira, A.S. Araújo, A.G.D. Santos, Formation of CeO_2 nanotubes through different conditions of hydrothermal synthesis, Surf. Interfaces 21 (2020) 100746.

[29] Y. Wang, L. Yin, A. Gedanken, Sonochemical synthesis of mesoporous transition metal and rare earth oxides, Ultrason. Sonochem. 9 (2002) 285–290.

[30] K. Polychronopoulou, A.F. Zedan, M.S. Katsiotis, M.A. Baker, A.A. AlKhoori, S.Y. AlQaradawi, S.J. Hinder, S. AlHassan, Rapid microwave assisted sol-gel synthesis of CeO_2 and $Ce_xSm_{1-x}O_2$ nanoparticle catalysts for CO oxidation, Mol. Catal. 428 (2017) 41–55.

[31] R. Li, S. Yabe, M. Yamashita, S. Momose, S. Yoshida, S. Yin, T. Sato, Synthesis and UV-shielding properties of ZnO- and CaO-doped CeO_2 via soft solution chemical process, Solid State Ionics 151 (2002) 235–241.

[32] J. He, L. Zhou, J. Liu, L. Yang, L. Zou, J. Xiang, S. Dong, X. Yang, Modulation of surface structure and catalytic properties of cerium oxide nanoparticles by thermal and microwave synthesis techniques, Appl. Surf. Sci. 402 (2017) 469–477.

[33] D.C. Marcano, D.V. Kosynkin, J.M. Berlin, A. Sinitskii, Z. Sun, A. Slesarev, L.B. Alemany, W. Lu, J.M. Tour, Improved synthesis of graphene oxide, ACS Nano 4 (2010) 4806–4814.

[34] P.S. Selvamani, J.J. Vijaya, L.J. Kennedy, A. Mustafa, M. Bououdina, P.J. Sophia, R.J. Ramalingam, Synergic effect of Cu_2O/MoS_2/rGO for the sonophotocatalytic degradation of tetracycline and ciprofloxacin antibiotics, Ceram. Int. 47 (2021) 4226–4237.

[35] J.W. Zhang, X. Zhang, Electrode material fabricated by loading cerium oxide nanoparticles on reduced graphene oxide and its application in electrochemical sensor for tryptophan, J. Alloy. Compd. 842 (2020) 155934.

[36] K. Kombaiah, J.J. Vijaya, L.J. Kennedy, M. Bououdina, B. Al Najar, Self heating efficiency of $CoFe_2O_4$ nanoparticles: a comparative investigation on the conventional and microwave combustion method, J. Alloy. Compd. 735 (2018) 1536–1545.

[37] H. Jan, M.A. Khan, H. Usman, M. Shah, R. Ansir, S. Faisal, N. Ullah, L. Rahman, The Aquilegia pubiflora (Himalayan columbine) mediated synthesis of nanoceria for diverse biomedical applications, RSC Adv. 10 (2020) 19219–19231.

[38] Z. Dong, B. Yang, H. Chang, L. Li, The fabrication and characterization of CeO_2/Cu_2O nanocomposites with enhanced visible-light photocatalytic activity, RSC Adv. 10 (2020) 36371–36377.

[39] K.K. Purushothaman, I.M. Babu, B. Saravanakumar, Hierarchical mesoporous $Co_xNi_{1-x}O$ as advanced electrode material for hybrid supercapacitors, Int. J. Hydrogen Energy 42 (2017) 28445–28452.

[40] X. Zhou, X. Shen, Z. Xia, Z. Zhang, J. Li, Y. Ma, Y. Qu, Hollow fluffy Co_3O_4 cages as efficient electroactive materials for supercapacitors and oxygen evolution reaction, ACS Appl. Mater. Interfaces 7 (2015) 20322–20331.

[41] R.R. Salunkhe, Y.V. Kaneti, Y. Yamauchi, Metal-organic framework-derived nanoporous metal oxides toward supercapacitor applications: progress and prospects, ACS Nano 11 (2017) 5293–5308.

[42] G. Zeng, Y. Chen, L. Chen, P. Xiong, M. Wei, Hierarchical cerium oxide derived from metal-organic frameworks for high performance supercapacitor electrodes, Electrochim. Acta 222 (2016) 773–780.
[43] C. Sengottaiyan, R. Jayavel, R.G. Shrestha, T. Subramani, S. Maji, J.H. Kim, J.P. Hill, K. Ariga, L.K. Shrestha, Indium oxide/carbon nanotube/reduced graphene oxide ternary nanocomposite with enhanced electrochemical supercapacitance, Bull. Chem. Soc. Jpn. 92 (2019) 521–528.
[44] J. Kim, C. Young, J. Lee, M.-S. Park, M. Shahabuddin, Y. Yamauchi, J.H. Kim, CNTs grown on nanoporous carbon from zeolitic imidazolate frameworks for supercapacitors, Chem. Commun. 52 (2016) 13016–13019.
[45] S. Britto, V. Ramasamy, P. Murugesan, B. Neppolian, T. Kavinkumar, Graphene based ceria nanocomposite synthesized by hydrothermal method for enhanced supercapacitor performance, Diam. Relat. Mater. 105 (2020) 107808.
[46] H. Qutaish, J. Lee, Y. Hyeon, S.A. Han, I.-H. Lee, Y.-U. Heo, D. Whang, J. Moon, M.-S. Park, J.H. Kim, Design of cobalt catalysed carbon nanotubes in bimetallic zeolitic imidazolate frameworks, Appl. Surf. Sci. 547 (2021) 149134.
[47] N. Kumar, M. Singh, A. Kumar, T.Y. Tseng, Y. Sharma, Facile and one-step in situ synthesis of pure phase mesoporous Li_2MnSiO_4/CNTs nanocomposite for hybrid supercapacitors, ACS Appl. Energy Mater. 3 (2020) 2450–2464.
[48] S. Nagamuthu, S. Vijayakumar, K.S. Ryu, Cerium oxide mixed $LaMnO_3$ nanoparticles as the negative electrode for aqueous asymmetric supercapacitor devices, Mater. Chem. Phys. 199 (2017) 543–551.
[49] L.J. Kennedy, T. Ratnaji, N. Konikkara, J.J. Vijaya, Value added porous carbon from leather wastes as potential supercapacitor electrode using neutral electrolyte, J. Clean. Prod. 197 (2018) 930–936.
[50] N. Maheswari, G. Muralidharan, Supercapacitor behavior of cerium oxide nanoparticles in neutral aqueous electrolytes, Energy Fuels 29 (2015) 8246–8253.
[51] E. Samuel, B. Joshi, Y. Il Kim, A. Aldalbahi, M. Rahaman, S.S. Yoon, ZnO/MnOx nanoflowers for high-performance supercapacitor electrodes, ACS Sustain. Chem. Eng. 8 (2020) 3697–3708.
[52] R. Kumar, A. Agrawal, R.K. Nagarale, A. Sharma, High performance supercapacitors from novel metal-doped ceria-decorated aminated graphene, J. Phys. Chem. C 120 (2016) 3107–3116.
[53] M. Mazloum-Ardakani, F. Sabaghian, M. Yavari, A. Ebady, N. Sahraie, Enhance the performance of iron oxide nanoparticles in supercapacitor applications through internal contact of α-Fe_2O_3@CeO_2 core-shell, J. Alloy. Compd. 819 (2020) 152949.
[54] D. Deng, N. Chen, Y. Li, X. Xing, X. Liu, X. Xiao, Y. Wang, Cerium oxide nanoparticles/multi-wall carbon nanotubes composites: facile synthesis and electrochemical performances as supercapacitor electrode materials, Phys. E: Low-Dimensional Syst. Nanostruct. 86 (2017) 284–291.